DOI: 10.13009/EUCASS2022-7286
9TH EUROPEAN CONFERENCE FOR AERONAUTICS AND SPACE SCIENCES (EUCASS)

Experimental study of the effect of a wavy surface in Taylor-Couette-Poiseuille flow

Lamia GAIED, Fethi ALOUI and Laurent KEIRSBULCK*

LAMIH UMR CNRS 8201, INSA Hauts-de-France, Université Polytechnique Hauts-de-France (UPHF)
Campus Mont Houy, F-59313 Valenciennes Cedex 9 – France

**Corresponding author e-mail: Fethi.Aloui@uphf.fr*

Abstract

In this article, we study the effect of an imposed axial flow on the Taylor-Couette flow with regularly distributed wavy form on the surface of the inner cylinder.
Without an imposed axial flow, a series of clearly distinguishable flow regimes develops; from the laminar flow Couette Flow CF to the vortex flow Wavy Taylor WVF, to the modulated flow Wavy Taylor Vortex MWVF and chaotic flows up to a full turbulence. Their appearance is highly dependent on the geometry of the CT system.
Furthermore, when an axial flow is imposed on a Taylor-Couette flow, new helical vortex structures are observed. The emergence of these flow states indicates that a richer dynamic can develop in CT flows. Hence, an imposed axial flow is an important factor / parameter in CT flow applications.
The superimposition of an axial flow can accentuate the dependence of the effect on surface roughness (form of the inner cylinder). It is interesting to note that the presence of a rough surface on the inner cylinder of the CTS accelerates the appearance of helical structures.
Using the visualization by Kalliroscope and the polarography technique, the time series of the velocity gradient obtained, were associated with each flow state, thus allowing the analysis and identification of the effect of an imposed axial flow on hydrodynamic instabilities' Couette-Taylor flow.

Keywords: Flow regimes, Critical Taylor Number, Wavy surface, Axial flow, Mass transfer, Wall shear stress.

NOMENCLATURE

A : Surface of the probe (m^2)
C : Concentration (mol/m^3)
d : Gap (mm)
D : Coefficient of diffusion ($m^2.s^{-1}$)
h : Height (mm)
I : Current (A)
l : Probe length
Pe : Péclet number
Re : Reynolds number
Re_{ax}: Axial Reynolds number
Ri : Inner cylinder radius (mm)
Ro : Outer cylinder radius (mm)
S : Wall shear stress (s-1)
Sh : Sherwood number
t : Time (s)
Ta : Taylor number
Ta_C : Critical Taylor number

Greek symbols
Γ : Aspect ratio (h/d)
Ω : Annular velocity of inner cylinder (rad/s)

DOI: 10.13009/EUCASS2022-7286

η : Radial ratio (Ri/Ro)
ϑ : Viscosity (m^2/s)

Subscripts
Lev : Lévêque approach
Sob : Sobolik et al. approach

1. Introduction

Couette Taylor flow is a prototype flow that develops in the gap between two coaxial cylinders. The inner cylinder is rotating and the outer cylinder is generally fixed.
The flow thus generated in the gap separating the two cylinders is very rich in dynamic instabilities. The study of different flow instabilities turns out to be interesting from a theoretical point of view. This system is well characterized by dimensionless numbers such as the Taylor Ta and Reynolds Re numbers, which are related.
In the Taylor-Couette-Poiseuille flow, an axial flow is imposed to the base flow. This Couette Taylor system has several applications such as sliding bearings, chemical reactors, biological separation devices and rotating machinery. Fénot et al. [1] were interested in heat transfer in TCPF.
Regarding chemical reactors, Kataoka et al. [2] proved the importance of characterizing this type of flow regime. In order to examine the influence of the superposition of an axial flow on the local mass transfer coefficients, they exploited the technique of electrodiffusion. The results illustrate that the axial flow causes a decrease in the mass transfer coefficient. Then, Resende et al. [3] inspected the phenomenon of mass transfer in a reactor. Poncet et al. [4] studied fluid flow and heat transfer in a narrow Taylor Couette-Poiseuille system with =η 0.961, based on Reynolds stress modelling.
Chandrasekhar [5] and DiPrima [6] studied the hydrodynamic stability of viscous flow between coaxial cylinders for a radius ratio close to 1. They have shown that the addition of axial flow to the base flow has a stabilizing effect. Indeed, the Taylor vortices appear at higher Taylor numbers compared to the case without axial flow. For Reynolds numbers greater than a critical value, the hypothesis of non-axisymmetric disturbances leads to the birth of pairs of helical vortices.
Giordano et al. [7] examined in their work the behaviour of vortex flow reactors in the region of progressive vortex flow, where non-corrugated toroidal vortices move downstream. They are interested in their studies at small axial Reynolds numbers, Re_{ax} (0.172-1.067). They showed that the core of the vortex slows down its axial displacement to increase the rotations of the inner cylinder.
Experimentally, Snyder [8], Schwarz et al. [9], Donnelly et al. [10] et Sorour et al. [11] have justified that at low Reynolds number, they note the appearance of toroidal translational vortices. While at higher Reynolds numbers helical vortices begin to appear.
Simmers et al. [12] et Lueptow et al. [13] used to characterize the flow, the ratio of the Taylor number to the axial Reynolds number, which describes the ratio of centrifugal accelerations to advective accelerations. Lueptow et al. [13] noted the pressure of the helical cells advancing in the same direction of the imposed axial flow. These structures have "a negative helix angle with respect to the direction of flow" (n = 1). For Reynolds numbers greater than 8, these structures were located in a narrow Taylor number domain near the Couette-Poiseuille flow. Then, the helical structures disappear and reappear in their place as wavy vortices, which always move in the same direction of axial flow for a higher Ta. Other authors [11] have noted other flow regimes. They found that at small Ta, wavy vortices and random wavy vortices exist. For Ta = 150 and Re = 6, they noticed in a very small region the birth of stationary helical structures with a negative n (-2).
Bühler [14] examined the Couette Taylor Poiseuille flow in a system, which is characterized by a radius ratio of 0.8. He obtained helical structures for values of n = -1, -2 and -3. For n = -1, these helical structures depend on the Reynolds number. They can be stationary as they can move up or down. However, for n = -2 and -3, the helical vortices are stationary.
Most studies focus on heat transfer for the case of rectangular cavities and only a few studies have been done on other forms of cavity geometry.
Recently, cylindrical channels with irregularities in the form of longitudinal cavities on the surface are widely adopted with the aim of improving heat transfer due to higher fluid mixing [15-18]. Indeed, the irregularities lead to the disturbance of the boundary layer therefore generates an increase in the thermal dissipation of the fluid close to the wall [19].
A numerical study was performed by Hayase et al. [20] on heat transfer in annular channels with irregularities on the inner and outer surfaces. They noted in the case of a cavity on the inner surface an improvement in heat transfer of up to 20% and up to 10% in the case of a cavity on the outer surface. Sommerer and Lauriat [21] carried out numerical research on the phenomenon of heat transfer in a ring, which is characterized by the presence of rectangular cavities

DOI: 10.13009/EUCASS2022-7286

on the outer surface. They noted that the number of cavities has an effect on improving the heat transfer inside the channels.
Experimentally, Fenot et al. [22] studied the influence of the inlet area on the heat transfer in annular channels with rotating inner cylinders which are characterized by longitudinal cavities. They noticed that the heat transfer is maximal in the area of the leading edge of the cavities. In other studies, Toghraie et al. [23] examined the effect of cavity dimensions on the heat transfer and pressure drop of nanofluids inside channels essentially the height of the cavity. The equations that characterize the problem have been discretized and solved numerically by adopting the finite volume method. They showed that the increase in the height of the internal cavities leads to a considerable improvement inside the microchannels of the heat transfer by convection and of the friction factor. Bilen et al. [24] experimentally studied the impact of the slit aspect ratio first on the heat transfer and second on the pressure drop of a fully developed turbulent air flow in several channels with different cavities. Jeng et al. [25] examined the effect of different axial cavity shapes on the inner cylinder rotating in the presence of axial airflow. They noted an increase in heat transfer by a factor of 1.4.
Numerically and experimentally, Lancial et al. [26] analysed the heat transfer as well as the temperature distribution on the rotor with cavity for laminar and turbulent air flows. They noticed that near the downstream end of the rotor notch, there is a hot spot. They also noted that due to the growth of the thermal boundary layers, the heat transfer coefficient on the pole face and in the notch, region decreases with increasing z. Experimentally, Nouri-Borujerdi and Nakhchi [27–29] investigated the impact of the assembly of cavities on the external fixed cylinder on the heat transfer as well as on the pressure drop of the annular flow between two cylinders. They marked correlations of the Nusselt number and the pressure drop linking the axial Reynolds number, the Taylor number, the number of cavities and their aspect ratio. They concluded that the ratio between heat transfer and pressure drop is maximum for a cavity aspect ratio of b/c=1.42.
Other types of cavities have been used. Skullong et al. [30] analysed the phenomenon of heat transfer in a solar air heater channel by adopting wavy cavities. They showed that the cavity pitch ratio parameter has an impact on improving the heat transfer of solar air heaters. Abou-Ziyan et al. [31] were interested in a study heat transfer by convection in an annular channel by placing interrupted helical fins on an inner cylinder which is in rotation. They deduce that the shape of the cavity has an impact on the improvement of the heat transfer inside the rotating annular channels. Zhu et al. [32] analysed the effect of the superposition of longitudinal cavities with triangular cross-section on the external fixed surface on the fluid flow inside the rotating annular channels. When the height of the cavity is less than the thickness of the boundary layer, the torque is the same as that of smooth surfaces.
Two types of surfaces (smooth surface, surface with irregularities) were used. The aim of this work is to examine the effect of surface irregularities on the velocity field for a cylindrical Couette flow with an imposed axial flow. Measurements by polarography for the Couette flow were carried out in this article.

2. Experimental setup

2.1. Taylor-Couette facility

The experimental system was typically designed in the study of a Taylor-Couette flow. A detailed sketch and photograph of this installation are given in Figure 1.

Figure 1: Experimental installation: Photography of the installation

DOI: 10.13009/EUCASS2022-7286

It consists of two coaxial cylinders that create a space occupied by a working fluid (in our case water). The inner cylinder can rotate through the use of an α-Step motor (marketed by the Omeron company). The outer plexiglass cylinder is fixed. The system is closed at the upper and lower ends with covers. The radii of the inner and outer cylinders are respectively R_i= 90 mm and R_o =100 mm, which gives a gap d = $R_o - R_i$ =10 mm and a gap ratio of η = R_i/R_o =0.9. The height of the cylinders is h =450 mm, which gives an axial aspect ratio of Γ=h /d =45.
All the results of this study relate to rotor/stator configurations, whose outer cylinder was kept fixed while varying the rotation of the inner cylinder.
The parameter that characterizes the dynamics of the flow is the Taylor number and the axial Reynolds number which are defined as:

$$\mathrm{Re} = \frac{\tau_\upsilon}{\tau_a} = \frac{\Omega \cdot R_i \cdot d}{\upsilon}$$

$$Ta = \frac{\tau_\upsilon}{\tau_{cent}} = \frac{\Omega \cdot R_i \cdot d}{\upsilon}\sqrt{\frac{d}{R_i}} = \mathrm{Re}\cdot\sqrt{\frac{d}{R_i}}$$

2.2. Geometry of the inner cylinder

Our objective is to evaluate the action of axial undulations on the behavior of Taylor-Couette flow, more precisely to identify possible mechanisms responsible for the increase in flow resistance. Thus, this configuration was compared to a reference cylinder having a smooth surface.
Figure 2 shows the inner cylinder configuration adopted. As can be seen, the outer cylinder is smooth and the inner cylinder has identical axial undulations which are arranged periodically.
The detailed shape of the corrugation is shown in Figure 2.
The depth, the shape of the roughness and the number of irregularities are generally used as key parameters to differentiate the different configurations of wall roughness.
In our case, the depth of the irregularities is equal to k = 3 mm. The surface of the corrugated cylinder is provided with 18 identical axial corrugations.

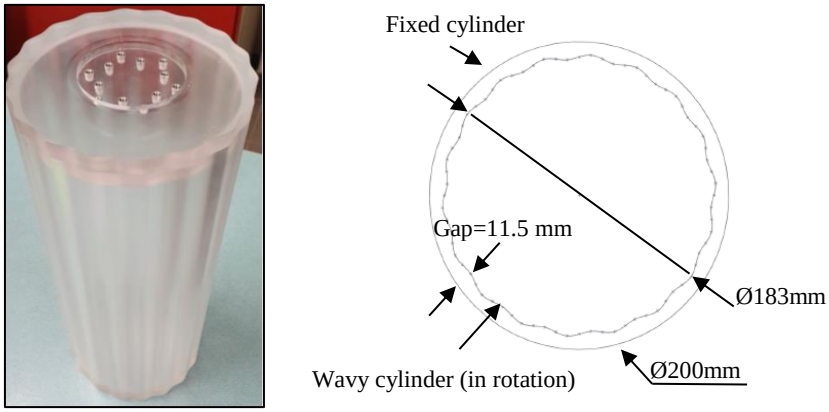

Figure 2: Geometry of the inner cylinder

3. Measurement methods

3.1. Visualization by Kalliroscope

The Kalliroscope is generally used to visualize flows. This product is a suspension formed of flakes of reflective ellipsoidal shapes, of dimensions 30x6x0.07 µm (Matisse and Gorman, 1984; Abcha, 2007) and of density 1.62 g/cm^3. It has a two-dimensional anisotropy. The Kalliroscope particles dispersed in the solution (approximately 1% to 2%) have a high refractive index equal to 1.85 which makes them easily visible, even in highly dilute solutions (less than 0.1%). The flakes align in the direction of the streamlines thus revealing the structure of the flow. The flow is visible if the particle has time to orient itself properly. The low concentration of particles avoids affecting the flow.

DOI: 10.13009/EUCASS2022-7286

3.2. Electrochemical method: Polarography

The polarography technique is an electrochemical or electro-diffusion method for measuring the parietal velocity gradient. This non-intrusive method focuses on the electro-diffusion aspect of matter, and more specifically on the oxidation-reduction reaction. The chemical reaction equation is written:

$$Fe(CN)_6^{3-} + e^- \Leftrightarrow Fe(CN)_6^{4-}$$

By applying a certain electric potential, the electric current that is generated is dependent on the concentration of the reactants and the mass transfer. The measurement of the mass transfer will make it possible to go back to the measurement of the parietal velocity gradient and thus to identify the imprint of a vortex on a wall.
A series of platinum probes were implanted on the inner surface of the outer cylinder of the Couette Taylor system (Figure 3).

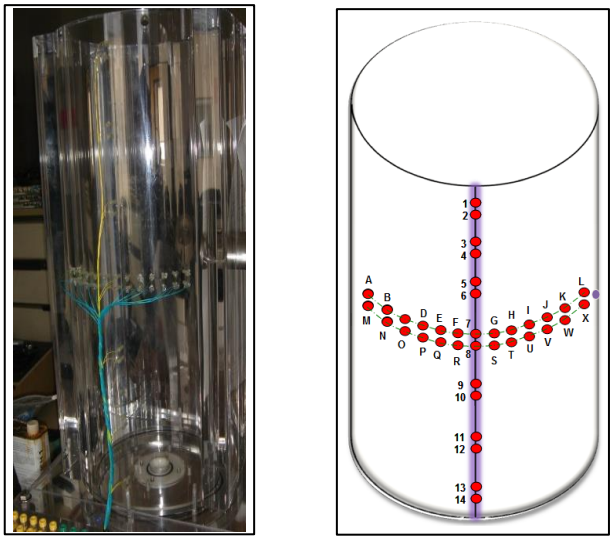

Figure 3: Electrochemical probes arrangement on the inner wall of the outer cylinder

3.3. PIV

The PIV (Particle Image Velocimetry) technique is a non-intrusive experimental technique, allowing the visualization and analysis of the flow. Thanks to a laser source illuminating at a very short interval a thin seeded layer of fluid and a CCD digital camera, PIV allows the reconstitution of instantaneous flow velocity fields.

4. Results and discussion

Flow regimes without and with axial flow

Various flow regimes were observed in the studied range of Re_{ax} (0, 32) and Ta (45, 319) are shown in Figures 4 to 14.

Taylor Vortex Flow without and with an axial flow

The rotation of the inner cylinder of the Couette-Taylor device (fixed outer cylinder) creates a flow at the level of the annular space between these two coaxial cylinders which form the test section. By gradually increasing this speed of rotation of the mobile cylinder, the first vortex structures begin to appear from the ends of the latter going all along the air gap of the two cylinders. For the case where the inner cylinder is wavy, Taylor vortices first appear near the ends of the cylinders at higher values of Ta than in the smooth case. The visualization of the flow by kalliroscope particles seeding the fluid and illuminated by a laser highlights the periodic movement forming vortex structures in the form of toroidal vortices (Taylor rollers). Visualization of the laser plane perpendicular to the flow plane in the gap of the Couette-Taylor device makes it possible to clearly distinguish the Taylor cells and thus to determine their number over the entire height of the test gap.

DOI: 10.13009/EUCASS2022-7286

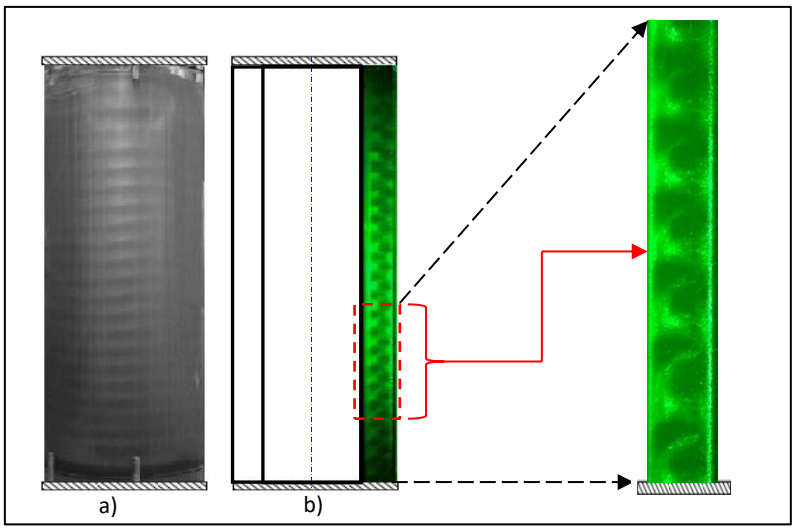

Figure 4: Taylor vortex regime Ta≈75:
a) Global visualization of Taylor vortices
b) Plane laser cut of the Taylor vortices

The axial wavelength is determined from the number of cells visualized and the height of the SCT. This visualization allowed us to determine the axial wavelength of periodic instabilities, which is approximately λ≈22 mm; i.e., λ≈2.2.d where d is the thickness of the gap (d=10mm). Figure 4 gives the general visualization of the TVF regime (figure (4-a)) as well as a sectional view of the Taylor cells by means of a normal section by a laser plane of the flow in the air gap.

We carried out a series of measurements by PIV in the Couette basic flow regime, in the Taylor roll regime and in the undulating Taylor roll regime to qualify our experimental device. Two-dimensional PIV measurements lead to errors due to the three-dimensional effect of the flow. This error becomes more significant when the thickness of the laser beam is large. The thickness of the laser beam should ideally be of the same order of magnitude as the seed particles. However, in practice, this is difficult to achieve. In our case study, we succeeded in achieving a thickness of the laser beam of the same order of magnitude as the particles. The PIV databases are recorded and post-processed in Matlab® to determine and analyze the velocity fields.

The smaller the PIV interrogation area, the better the accuracy of the near-wall velocity vector fields. The interrogation area is then chosen small; which made it possible to get as close as possible to the zone close to the wall.

The PIV measurements allowed us to determine the instantaneous velocity fields along the air gap. In the case where the inner cylinder is wavy, the velocity field for a Taylor number respectively equal to Ta =45 and Ta =75 show the development of vortex structures along the gap characterizing the Taylor roll regime (TVF).

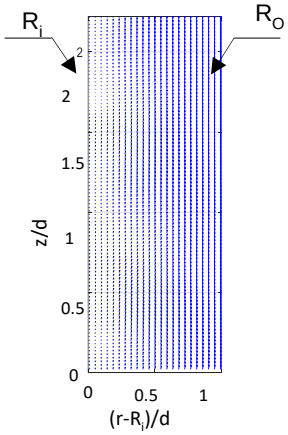

Figure 5: Velocity field determined by PIV at Ta =45 (wavy inner cylinder)

DOI: 10.13009/EUCASS2022-7286

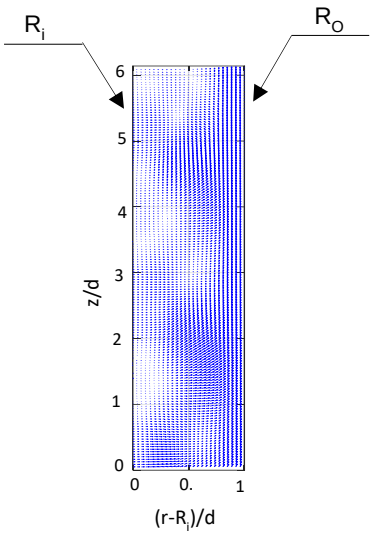

Figure 6: Velocity field determined by PIV at Ta =75 (wavy inner cylinder)

The line on the left at each instant represents the rotating inner cylinder (Wavy) (R_i) and the line on the right represents the stationary outer cylinder (R_O). The vortex centres are well marked in Figure 6. The experimental results show that the alternation of the velocity field for different Taylor numbers proves well the axial periodicity of the flow in the form of pairs of counter-rotating Taylor cells. These toroidal vortices (Taylor rolls) are characterized by an axial periodicity of wavelength $\lambda \approx 2.2d$. There is a stretch in the inflow region and a tightening of the velocity lines in the outflow region. This is due to the asymmetry of the flow generated by the oscillations of the separators. It is induced by the transfer of fluid from the adjacent vortex to the adjacent vortex of the same pair.

We carried out a series of Taylor flow tests at the threshold (appearance of the TVF regime) and after the threshold with an imposed axial flow. Each time, the Taylor roll flow being developed, we then impose the axial flow. The evolutions of the Couette-Taylor-Poiseuille flow for $Ta \approx 75$, superimposed on an axial flow characterized respectively by an axial Reynolds number $Re_{ax} \approx 0.5$, $Re_{ax} \approx 3$ and $Re_{ax} \approx 18$ are illustrated in Figure 7.
At $Re_{ax} = 0$, there is an alternation of signals which characterizes the presence of well-developed contra-rotating vortices.
Note that for low axial Reynolds numbers, A disordered flow that occurs at the bottom and regular Taylor vortices started at a distance of 1 cm from the bottom. Then, the Taylor vortices begin to move in the same direction as the imposed axial flow without disturbing their toric structure and an upward helix is formed. In the cases illustrated, the helical vortices rise at a rate of 1 to 1.3 the velocity of the axial flow. This confirms the results of Johnson and Lueptow [33]. By increasing the axial Reynolds number to $Re_{ax} \approx 18$; the propeller breaks and eventually disappears (Fig.7). The instability is then delayed in the presence of an axial flow corresponding to $Re_{ax} \approx 18.37$. This confirms the visualizations of Weisberg et al. [34].

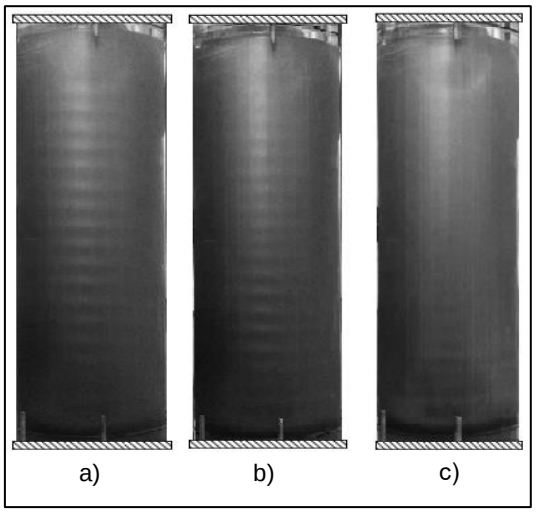

Figure 7: Couette-Taylor-Poiseuille regime for $Ta \approx 75$:
a) $Re_{ax} \approx 0.5$, b) $Re_{ax} \approx 3$, c) $Re_{ax} \approx 18$

DOI: 10.13009/EUCASS2022-7286

For an axial Reynolds number of about Re_{ax}=18, the helical vortices rise more rapidly in the direction of the axial flow and begin to break up at the base of the Couette-Taylor device (entrance of the axial flow). In this case of configuration, the axial flow takes over the Couette-Taylor flow on the lower part of the cylinders and the Taylor instability is then delayed.
Vortex structures tend to advect fluid that is characterized by high azimuthal momentum from near the inner cylinder outward and low azimuthal momentum fluid from near the outer cylinder inward.

The electro-diffusion measurements of the wall shear rate for Couette flow had several purposes. The first objective was to obtain a detailed spatio-temporal mapping of the wall shear rate at several Reynolds numbers. The second objective was to compare the wall shear rate without and with an axial flow for the case where the surface of the inner cylinder is corrugated. The wall shear rate was determined using two approaches. Indeed, the first approach of Levêque [35] is applicable in steady state, for high Péclet numbers and when axial diffusion can be neglected. It shows the relationship between the local and instantaneous mass transfer and the local and the instantaneous shear rate of the wall.

$$S_q = S_{Lev} = \frac{D}{l^2}\left(\frac{Sh(t)}{0.807}\right)^3$$

Sh : The Sherwood number i.e., the mass transfer rates time-evolution.

$$Sh(t) = \frac{I(t)\cdot l}{nFC_0AD}$$

The second approach is that of Sobolik et al. [36]. It is applicable for high average Péclet numbers when the sampling rate is sufficient. Sobolik et al. [36] introduced the term of the unsteady response of the ED probe multiplied by the time derivative of the mass transfer rate.

$$S_{Sob}(t) = S_q(t) + \frac{2}{3}\theta(t)\left(\frac{\partial S_q(t)}{\partial t}\right)$$

where:

$$\theta(t) = 0.486\,\ell^{\frac{2}{3}} D^{-\frac{1}{3}} S_q(t)^{-\frac{2}{3}}$$

The evolution of the parietal velocity gradient, obtained according to the Levêque method as a function of time, is illustrated by figure 8. It is noted that the two signals are completely in phase, since the determination of the gradient by this technique involves neither the attenuation of the mass transfer signal nor its phase shift. The method of Sobolik et al. (1987), which interacts with the correction of these two parameters, in fact makes it possible to remedy this problem as long as the amplitudes of fluctuations of the "parietal velocity gradient" signal remain less than or equal to 100% of its average.

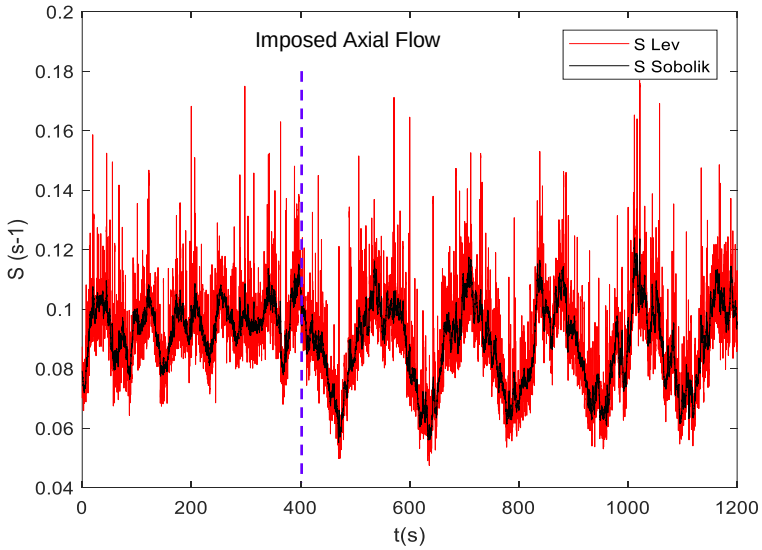

Figure 8: Evolution of wall shear rates for Taylor Vortex Flow TVF (Ta=75) imposed to an axial flow (Re_{ax} = 3.2) (probe 7)

DOI: 10.13009/EUCASS2022-7286

Thus, we can notice that the signals coming from the electrochemical probes for the TVF regime where Ta≈75, are periodic. By imposing an axial flow characterized by an axial Reynolds number Re_{ax}=3.2, the signal retains its wave character, but with an increase in the period of the signal. This can be interpreted by the stabilizing effect exerted by this axial flow.
In summary, the Couette-Taylor flow with axial flow can be likened to an annular Poiseuille flow with superposition of an azimuthal flow induced by a differential rotation of the cylinder, it corresponds to the spiral Poiseuille flow (spiral Poiseuille flow). Two kinds of instability (centrifugal instability, instability due to shear) can occur in this type of flow (Martinand, 2009). Their appearance depends on competition between the axial flow and the azimuthal flow (Meseguer and Marques, 2002).

Wavy Vortex Flow without and with an axial flow

This second instability is characterized by the appearance of an azimuthal wave superimposed on the first Taylor vortex rolls, thus generating their oscillation. Thus, the rollers take on a periodic wave shape around the cylinder in the azimuthal and axial direction, thus breaking the axisymmetricity of the rollers. These ripples are clearly visible thanks to the light reflections of the Kalliroscope particles (figure 9).

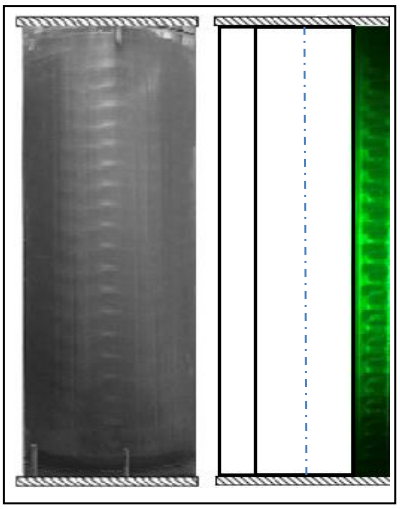

Figure 9: Flow visualization for the WVF regime for Ta=115

We also present in figure 10 the temporal evolutions of the parietal velocity gradient determined from the methods of Leveque and Sobolik (1987) for Ta=105 (probe 7). It shows that the azimuthal wavelength of the main wave is no longer homogeneous on the contour of the SCT.

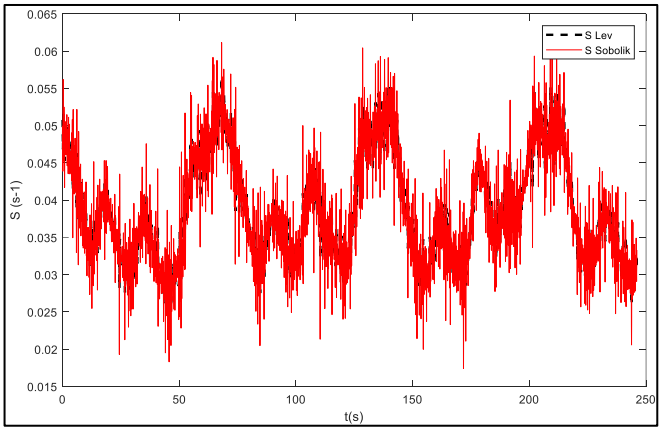

Figure 10: Example of temporal evolution of the parietal velocity gradient determined from the methods of Leveque and Sobolik (1987) for Ta=105 (probe 7)

Figure 10 illustrates an example of the temporal evolution of the parietal velocity gradient determined using the methods of Leveque and Sobolik (1987) for Ta=105 (probe 7). The development of wavy instabilities is clearly noticeable. The latter are represented for a Taylor number Ta=105 which corresponds to the first range of the wavy

DOI: 10.13009/EUCASS2022-7286

vortex regime (WVF). Wavy vortices are well marked by the presence of oscillations on the wall shear rate curve. Indeed, the amplitude and the offset of the oscillation necessarily depend on the positions of the probes on the CTS.
A vortex flow that is characterized by a predominant azimuthal wave was present at low T=105. We can also observe three small waves between two predominant waves. Thus, we distinguish a long period, which corresponds to the passage of a Taylor vortex and another short corresponding to the waves.

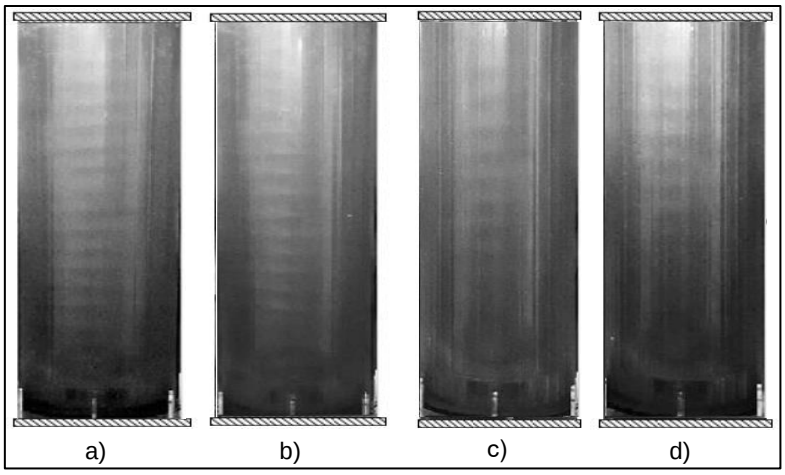

Figure 11: Couette-Taylor-Poiseuille flow for Ta=112:
a) Re_{ax}=3; b) Re_{ax}=21; c) Re_{ax}=32; d) Re_{ax}=53

Figure 11 illustrates the visualization of the flow in the WVF regime (Ta= 112) superimposed on an axial flow (Re_{ax}=3). It shows the presence of vortex structures. Axial flow is unable to block or break the development of wavy vortices. The vortices had an axial wavelength and they moved in the direction of the axial flow.
The visualizations show that by increasing the rate of the axial flow compared to the previous case (Re_{ax}=3) Re_{ax}< 21, and by superimposing a flow in the WVF regime, the wavy vortices are formed despite the presence of a high axial flow. Wavy Taylor vortices persist inside, even at relatively high axial flow rates.
At average values of the Reynolds number Re and the low Taylor number Ta, we note the birth of a helix which winds in the opposite direction of the basic flow.
We can note here that an important imposed axial flow allows the destabilization of the WVF regime. Detached structures arise and give a destabilizing character to the resulting flow.
The temporal evolution of the wall shear rate for Ta=112 before and after superimposition of an axial flow Re_{ax}=21 is presented in Figure 12. By imposing an axial flow on the basic wavy vortex flow, the period corresponds to the passage of a pair of vortices increases (figure 12). As well as without axial flow, the shear rate had values between 0.19 s^{-1} and 0.195 s^{-1}. Whereas with axial flow it varies between 0.18 s^{-1} and 0.22 s^{-1}. The shear rate maxima were less than Re_{ax}=21 due to the stabilizing effect of the superimposition of the axial flow on the base flow.

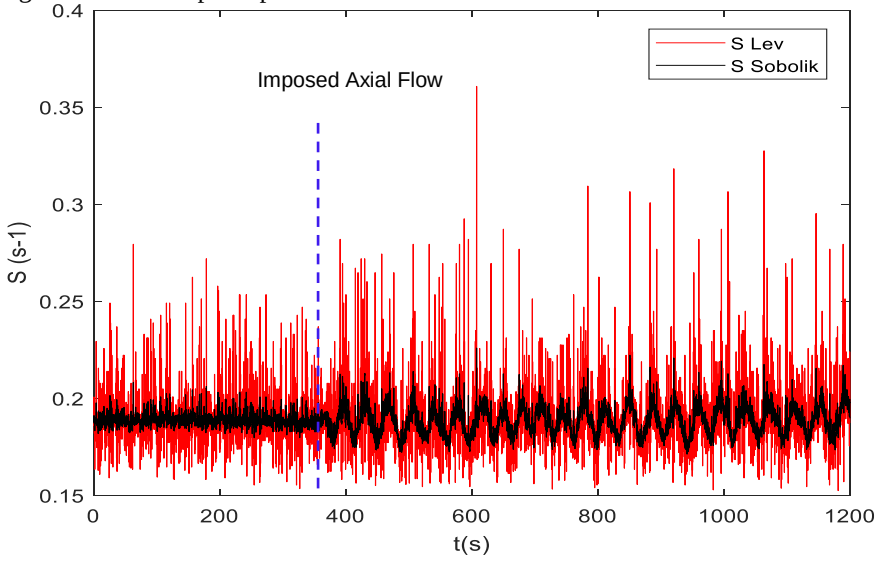

Figure 12: Evolution of wall shear rates for Wavy Vortex Flow
WVF (Ta=112) imposed to an axial flow (Re_{ax} = 21) (probe 7)

DOI: 10.13009/EUCASS2022-7286

The variation of the shear rate of the wall had been always positive because it reflected the rotation (of the structures) around the axis of the cylinder. The maximum and minimum values of the shear rate of the wall are located respectively in the exit and entry regions of the Taylor vortices.
We can note then, by increasing the Reynolds number, we note the disappearance of the small waves and the profile of the parietal shear rate has become more regular. The superposition of an axial flow Re_{ax} >53 generates the overlap, the stretching and then the breaking of the vortices (Figure 11). The flow becomes then axial. The axial flow is not able to slow down the formation of the corrugated vortices or to break them. The effect of the flow azimuth wins.

Modulated Wavy Vortex Flow without and with an axial flow

Figure 13 illustrates the visualizations resulting from the superposition of an axial flow (Re_{ax}=30, Re_{ax}=52 and Re_{ax}=74) on a MWVF flow (Ta=180).

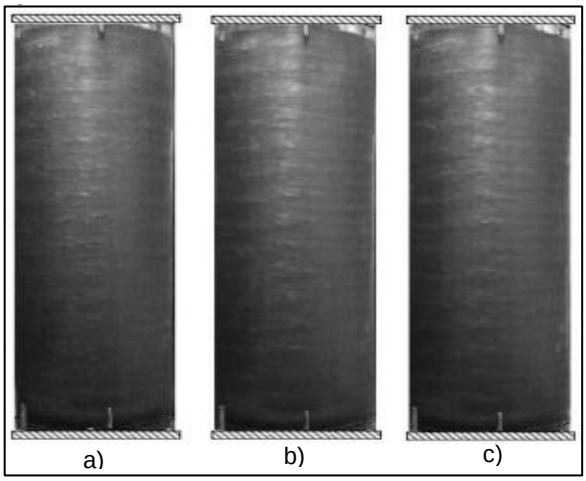

Figure 13: Couette-Taylor-Poiseuille flow for Ta=180:
a) Re_{ax}=30; b) Re_{ax}=52; c) Re_{ax} =74

Figure 13 shows that for an axial flow corresponding to Re_{ax} = 74 superimposed on the initial flow (Ta = 180), we note the appearance and development of vortices at inside that move in the direction of axial flow. Despite the large axial flow, vortices appear and develop along the gap of the system. They are characterized by turbulent structures inside. A high axial flow imposed on the base flow may have a stabilizing effect on the occurrence of the MWVF.

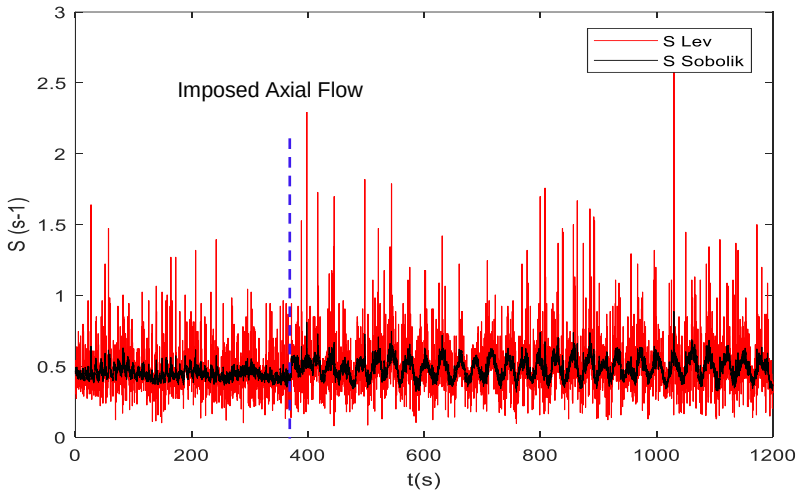

Figure 14: Evolution of wall shear rates for Modulated Wavy Vortex Flow
MWVF (Ta=183) imposed to an axial flow (Re_{ax} = 32) (probe 7)

For Ta=183 (MWVF), the signal present repetitive sinusoidal shapes characterized by two neighboring sinusoids. Moreover, the periods are lower compared to that of the signal corresponding to the WVF regime. The superimposition of an axial flow (Re_{ax} = 32) caused an increase in the period of the signal produced. This can be interpreted by the stabilizing effect exerted by this axial flow despite the predominance of the centrifugal effect resulting in the regeneration of instabilities in the air gap.

DOI: 10.13009/EUCASS2022-7286

3. Conclusion

Couette-Taylor-Poiseuille flow dynamics have been studied at several axial Reynolds numbers and Taylor numbers. Visualizations by kalliroscope particles and polarographic measurements were performed for different surfaces used to study the influence of the superposition of an axial flow on the base flow.
In this study, we are interested in the effect of surface irregularities on the birth of helical structures which is due to the imposed axial flow.
For a low imposed axial flow, the latter leads to a stabilization of the developed flow. Note that for low axial Reynolds numbers, the Taylor vortices begin to move in the same direction as the imposed axial flow and an upward helix is formed.
In summary, visualizations show that an axial flow imposed on a TVF flow has a flow stabilizing effect for a Reynolds number interval Re_{ax} <18.37. Axial flow delays the onset of instability corresponding to the transition to the WVF regime.
With an important axial flow ($Re_{ax} \approx 100$), the latter is sufficient to break up the MWVF vortex, but is unable to destabilize the nascent turbulent regime where the vortices still exist along the gap. Then, due to the superposition of the axial flow, the vortices are more dispersed.

Acknowledgments

This work was supported by the laboratories LAMIH (UMR CNRS 8201) of Polytechnic University Hauts-de-France (INSA Hauts-de-France; Valenciennes, France) and GEPEA UMR CNRS 6144 (Nantes University, France). These supports are gratefully acknowledged.

References

[1] Fénot, M., Bertin, Y., Dorignac, E., Lalizel, G. A. 2011.Heat transfer between concentric rotating cylinders with or without axial flow. Int J Thermal Sci. 2011; 50: 1138–1155.
[2] Kataoka, K., Doi, H., Komai, T. 1977. Heat/Mass transfer in Taylor vortex flow with constant axial flow rates. Int J Heat Mass Transfer. 1977; 20: 57–63.
[3] Resende, MM., Vieira, PG., Sousa, R Jr., Giordano, RLC., Giordano, RC., "Estimation of mass transfer parameters in a Taylor-Couette-Poiseuille heterogenous reactor", Brazilian J Chem Engng. 2004; 21: 175– 184 (2004).
[4] Poncet, S., Haddadi, S., Viazzo. 2011.Numerical modelling of fluid flow and heat transfer in a narrow Taylor Couette-Poiseuille system. Int J Heat Mass Transfer. 2011; 32: 128–144.
[5] Chandrasekhar, S. 1960. The hydrodynamic stability of viscid flow between coaxial cylinders. Proc Nat Acad Sci. 1960; 46: 141–151. PMID: 16590590.
[6] DiPrima, RC. 1960. The stability of a viscous fluid between rotating cylinders with an axial flow. J Fluid Mech. 1960; 9: 621–631.
[7] Giordano, R. C., Giordano, R. L. C., Prazeres, D. M. F., Cooney, C. L. 1998. Analysis of a Taylor–Poiseuille vortex flow reactor. I: Flow patterns and mass transfer characteristics. Chem. Eng. Sci. 53, 3635.
[8] Snyder, H. A. 1962. Experiments on the stability of spiral flow at low axial Reynolds numbers. Proc. R. Soc. London, Ser. A 265, 198.
[9] Schwarz, K. W., Springett, B. E., and Donnelly, R. J. 1964. Modes of instability in spiral flow between rotating cylinders. J. Fluid Mech. 20, 281.
[10] Donnelly, R. J., and Fultz, D. 1960. Experiments on the stability of spiral flow between rotating cylinders. Proc. Natl. Acad. Sci. USA 46, 1150.
[11] Sorour, M. M., and Coney, J. E. R. 1979. The characteristics of spiral vortex flow at high Taylor numbers. J. Mech. Eng. Sci. 21, 65.
[12] Simmers, D. A., and Coney, J. E. R. 1979. The experimental determination of velocity distribution in annular flow. Int. J. Heat Fluid Flow 1, 177.
[13] Lueptow, R. M., and Hajiloo, A. 1995. Flow in a rotating membrane plasma separator. Am. Soc. Artif. Int. Organs J. 41, 182.
[14] Bühler, K. 1984. Instabilitäten spiralförmiger Strömungen im Zylinderspalt. ZAMM—J App Math Mech. 1984, 64: 180–184.
[15] Naresh, Y., Balaji, C., Thermal performance of an internally finned two phase closed thermosyphon with refrigerant R134a: a combined experimental and numerical study, Int. J. Therm. Sci. 126 (2018) 281–293.

[16] Zheng, N., Liu, P., Shan, F., Liu, Z., Liu, W., Turbulent flow and heat transfer enhancement in a heat exchanger tube fitted with novel discrete inclined grooves, Int. J. Therm. Sci. 111 (2017) 289–300.
[17] Córcoles-Tendero, J.I., Belmonte, J.F., Molina, A.E., Almendros-Ibáñez, J.A., Numerical simulation of the heat transfer process in a corrugated tube, Int. J. Therm. Sci. 126 (2018) 125–136.
[18] Xu, W., Wang, S., Liu, G., Zhang, Q., Hassan, M., Lu, H., Experimental and numerical investigation on heat transfer of Therminol heat transfer fluid in an internally fourhead ribbed tube, Int. J. Therm. Sci. 116 (2017) 32–44.
[19] Ravi, B.V., Singh, P., Ekkad, S.V., Numerical investigation of turbulent flow and heat transfer in two-pass ribbed channels, Int. J. Therm. Sci. 112 (2017) 31–43.
[20] Hayase, T., Humphrey, J., Greif, R., Numerical calculation of convective heat transfer between rotating coaxial cylinders with periodically embedded cavities, J. Heat Tran. 114 (1992) 589–597.
[21] Sommerer, Y., Lauriat, G., Numerical study of steady forced convection in a grooved annulus using a design of experiments, J. Heat Tran. 123 (2001) 837–848.
[22] Fénot, M., Dorignac, E., Giret, A., Lalizel, G., Convective heat transfer in the entry region of an annular channel with slotted rotating inner cylinder, Appl. Therm. Eng. 54 (2013) 345–358.
[23] Toghraie, D., Karimipour, A., Safaei, M.R., Goodarzi, M., Alipour, H., Dahari, M., Investigation of rib's height effect on heat transfer and flow parameters of laminar water–Al2O3 nanofluid in a rib-microchannel, Appl. Math. Comput. 290 (2016) 135–153.
[24] Bilen, K., Cetin, M., Gul, H., Balta, T., The investigation of groove geometry effect on heat transfer for internally grooved tubes, Appl. Therm. Eng. 29 (2009) 753–761.
[25] Jeng, T.-M., Tzeng, S.-C, Lin, C.-H., Heat transfer enhancement of Taylor–Couette–Poiseuille flow in an annulus by mounting longitudinal ribs on the rotating inner cylinder, Int. J. Heat Mass Tran. 50 (2007) 381–390.
[26] Lancial, N., Torriano, F., Beaubert, F., Harmand, S., Rolland, G., Study of a Taylor-Couette-Poiseuille flow in an annular channel with a slotted rotor, Electrical Machines (ICEM), 2014 International Conference on IEEE, 2014, pp. 1422–1429.
[27] Nouri-Borujerdi, A., Nakhchi, M.E., Optimization of the heat transfer coefficient and pressure drop of Taylor-Couette-Poiseuille flows between an inner rotating cylinder and an outer grooved stationary cylinder, Int. J. Heat Mass Tran. 108B (2017) 1449–1459.
[28] Nouri-Borujerdi, A., Nakhchi, M.E., Heat transfer enhancement in annular flow with outer grooved cylinder and rotating inner cylinder: review and experiments, Appl. Therm. Eng. 120 (2017) 257–268.
[29] Nouri-Borujerdi, A., Nakhchi, M.E., Experimental study of convective heat transfer in the entrance region of an annulus with an external grooved surface, Exp. Therm. Fluid Sci. 98 (2018) 557–562.
[30] Skullong, S., Promvonge, P., Thianpong, C., Pimsarn, M., Thermal performance in solar air heater channel with combined wavy-groove and perforated-delta wing vortex generators, Appl. Therm. Eng. 100 (2016) 611–620.
[31] Abou-Ziyan, H.Z., Helali, A.H.B., Selim, M.Y., Enhancement of forced convection in wide cylindrical annular channel using rotating inner pipe with interrupted helical fins, Int. J. Heat Mass Tran. 95 (2016) 996–1007.
[32] Zhu, X., Ostilla-Mónico, R., Verzicco, R., Lohse, D., Direct numerical simulation of Taylor–Couette flow with grooved walls: torque scaling and flow structure, J. Fluid Mech. 794 (2016) 746–774.
[33] Johnson E. C., Lueptow R. M., Hydrodynamic stability of flow between rotating porous cylinders with radial and axial flow‖, Phys. Fluids, (1997) Vol. 9, 3687.
[34] Weisberg A., Smits A.J., Kevrekidi I., Delaying transition in Taylor-Couette flow with axial motion of the inner cylinder, J. Fluid Mech., (1997) Vol. 11, 1.
[35] Lévêque M.A., Les lois de transmission de la chaleur par convection, Ann. Mines, (1928) Vol. 13, 381-412.
[36] Sobolik V., Wein O., J. Cermak, Simultaneous measurement of film thickness and wall shear stress in wavy flow of non-Newtonian liquids, Collection Czechoslovak Chem. Comun., (1987) Vol. 52, 913-928